Chemical Papers (2022) 76:373–384
https://doi.org/10.1007/s11696-021-01866-7

ORIGINAL PAPER

Anti-metastatic cancer activity of ultrasonic synthesized reduced graphene oxide/copper composites

Ahmad S. Kodous[1] · M. M. Atta[2] · Gehan R. Abdel-Hamid[1] · H. A. Ashry[2]

Received: 17 July 2021 / Accepted: 7 September 2021 / Published online: 15 September 2021

Abstract

In this paper, different nanocomposites based on copper metal particles (Cu) grown on reduced graphene oxide (RGO) were synthesized by the cost-effective, one-step, and facile sonochemical approach. The prepared nanocomposites were applied as an anticancer agent for breast cancer cell lines (MCF-7). The sonication of graphene oxide (GO) solution in the presence of Cu transformed it into RGO. By varying Cu concentration (x) in GO solution, series of RGO/Cux nanocomposites were obtained (where x = 15, 30, and 50%). The reduction degree of RGO was dependent on Cu concentration, as revealed by XRD and FTIR. Raman spectroscopy revealed the increased defect level of RGO/Cu nanocomposites compared to GO. From TGA, the thermal stability of nanocomposites was increased by increasing Cu concentration. The smooth GO sheets were restacked upon the incorporation of Cu, as shown by SEM. The size of Cu nanoparticles size was decreased upon sonication, as revealed by HRTEM. It found that all prepared RGO/Cu nanocomposites have MCF-7 inhibition, but RGO/Cu30 shows the most inhibition. Also, the gene expressions of Cathepsin D, MMP9, and Bcl-2 decreased, and p53 increased by RGO/Cu30, which induced anti-metastatic activity and apoptosis in MCF-7 cells. RGO/Cu30, we concluded, can be employed as an anti-metastatic agent by inhibiting Cathepsin D and MMP9, as well as an anticancer agent by inducing P53 and inhibiting Bcl-2 expression.

Keywords Anti-metastatic · Copper · Graphene oxide · Ultrasound irradiation · Cathepsin D · Gene expression

Introduction

Since the discovery of graphene, many researches have been done on graphene due to its exclusive properties. The excellent chemical and physical properties of graphene and graphene-based materials had attracted scientific community attention in the applications such as supercapacitors, polymer processing, photocatalysis, sensors, heavy metal absorbance, and composite materials (Moussa et al. 2011; Novoselov et al. 2005; Stankovich et al. 2006; Schedin et al. 2007; Singh et al. 2011; Goldsmith et al. 2019; Ai et al. 2019; Strauss et al. 2018; Ahmed et al. 2021; Atta et al. 2021a).

Also, scientists studied graphene's biological properties and they found that it is a very good material for the production of scaffolds (Pinto et al. 2013; Jakus et al. 2015), implants (Bitounis et al. 2013), biosensors, tissue engineering, and drug carrier (Shadjou et al. 2018; Lu 2019; More et al. 2019).

Graphene applications also extended to be used as anticancer material depending on its low toxicity, can induce apoptosis, local action, and a less ability to move (Zhang et al. 2019; Yang et al. 2013). As well as, graphene surface properties allow bind several nanomolecules like gold, silver, copper, and quantum dots, which in turn enhance therapeutic and imaging techniques (Rahman et al. 2019).

There are several graphene preparation methods, such as epitaxial growth (Sutter 2009), mechanical exfoliation (Yi and Shen 2015). Although low quality of produced graphene, the reduction method of GO is the most recognized for graphene preparation regarding the cost and large scale production (Pei and Cheng, 2012). This method includes

✉ M. M. Atta
mohatta2014@gmail.com; mohamed_atta@eaea.org.eg

[1] Radiation Biology Department, National Center for Radiation Research and Technology (NCRRT), Egyptian Atomic Energy Authority (EAEA), Cairo, Egypt

[2] Radiation Physics Department, National Center for Radiation Research and Technology (NCRRT), Egyptian Atomic Energy Authority (EAEA), Cairo, Egypt

graphite oxidation to obtain GO as the first step, and the second step is GO reduction. The reduction may be performed chemically, thermally, or by irradiation (McAllister et al. 2007; Zhang et al. 2012; Atta et al. 2021b).

Cancer is the most serious health problem worldwide (Huma et al. 2019). It was expected that 20–30 million new cancer cases and 13–17 million people would die from cancer worldwide by 2030 (Katikireddi and Setty 2013). Because of the high death rate associated with cancer and the serious chemotherapy and radiotherapy side effects, it is of great interest to find novel anticancer agents.

Recently, the researchers were focused on the metals as anticancer because they exhibit less toxicity and exhibit more tumor antiproliferative activity (Sorenson 1992; Studer et al. 2010).

Transition metal complexes have been broadly studied for their activity, like nuclease using the metal and dioxygen redox properties to yield reactive oxygen species to induce DNA cleavage by base modification or direct strand scission (Burrows and Muller 1998). Recently, metal nanoparticles such as gold, silver, and copper have been tested as anticancer agents (Jain et al. 2012; Wei et al. 2015; Jose et al. 2011).

The copper (Cu) complex compounds have proved to have varied anticancer activity due to the broad-spectrum anticancer activities (Santini et al. 2013), the selective membrane permeability of cancer cells to copper compounds. Besides, copper has longer stability and low cost than gold and silver (Metcalfe and Thomas 2003; Laha et al. 2014). The development of nanocomposites that combine a carbon-based material and metal particles enhances anticancer due to their high surface area, the excellent stronger inhibitory effect (Hu et al. 2012). Furthermore, copper and its alloys have been used for antibacterial purposes practically since their discovery, even before discovered illnesses microbial nature. Copper is an important trace metal for flora and fauna, although it is poisonous to some bacteria, unlike lead, which was once employed for similar purposes (Dobrovolný et al. 2017).

The nanocomposites synthesis and modification by high-intensity ultrasound irradiation technique (sonochemical) received great attention due to its advantages. It provides energy efficiency, homogeneity, ease, low cost, fast reaction kinetics, and low pressure needed for reactions (Hunge et al. 2019). The high-energy ultrasound produced by cavitation provides implosive collapsing bubbles in the reaction medium resulting in radicals that initiate the reaction (Xu et al. 2013).

In the present work, nanocomposites that consist of reduced graphene oxide (RGO) incorporated with different ratios of Cu were prepared sonochemically as a simple and fast method. Herein, Cu metal particles act as a reducing agent to convert GO into RGO. The effect of different loading of Cu particles on structural and thermal properties of obtained RGO was studied. The anticancer activity of different RGO/Cu for Breast cancer cell lines (MCF-7) was tested. Evaluation of the expression of four genes Cathepsin D, MMP-9, Bcl-2, and p53 in vitro cell culture exposed to the most RGO/Cu complex exhibit inhibition carried out.

Materials and methods

Materials

Graphite (< 50 μm) was procured from Merk, Germany. H_2SO_4 (98%), H_3PO_4 (85%), and Hydrazine hydrate were purchased from Sigma-Aldrich, USA. $KMnO_4$, H_2O_2 (35%), ethanol (96%), and HCl purchased were from El Nasr Pharmaceutical chemicals Company, Egypt. Copper was purchased from BDH Chemicals Ltd, England. EAC cell lines originally derived from mammary gland tumors and breast cancer cell lines (MCF-7) were obtained from the National Cancer Institute (NCI), Cairo University. Dulbecco's modified eagle medium (DMEM), fetal bovine serum (FBS), 3-(4, 5-di-methyl-2-thiazolyl)-2, 5-diphenyl-2Htetrazolium bromide (MTT), streptomycin, penicillin, and deionized water were obtained from Sigma-Aldrich. RNeasy mini kit was obtained from Quick-RNA™, Germany. The RNA to-cDNA™ kit was obtained from Applied Biosystems, USA. Taq-Man Fast Advanced Master Mix was obtained from Applied Biosystems StepOnePlus™ system.

Synthesis of graphene oxide

Graphene oxide (GO) prepared from commercial graphite based on improved Hummer's method (Marcano et al. 2010). Briefly, 1 g of graphite was dissolved in 100 ml solution mixture from $H_2SO_4 + H_3PO_4$ (3:1) in an ice bath. Then, 6 g of $KMnO_4$ were gradually added to the mixture, which was kept under continuous stirring for about 24 h. Then, the deionized water was added to the mixture. The color of the mixture was observed to turn from dark purplish-green to dark brown. Then, 30 ml of H_2O_2 solution was added to stop the oxidation process. The formed graphite oxide solid was washed with HCl aqueous solution and then washed with deionized water until a pH reaches up to 3.

Synthesis of reduced graphene oxide/copper (RGO/Cu) nanocomposites

Three samples each 200 mg of GO dissolved in 200 ml distilled water and ultrasonicated for about 1 h. The copper metal powder was added to the above mixture with concentrations of 15, 30, and 50% compared to GO weight, and then, the mixture was ultrasonicated for about 6 h. During the sonication process, the brown color of the GO/Cu solution turned into black color, which confirmed the

reduction in GO. The obtained complexes were precipitated and washed with distilled water. The obtained RGO/Cu samples were designated according to Cu percentage, i.e., RGO/Cu15, RGO/Cu30, and RGO/Cu50. A schematic representation for RGO/Cu nanocomposites synthesis is given in Fig. 1.

Characterization techniques

The structural analysis of the prepared samples was carried out by X-ray diffractometer (XRD, Shimadzu) using CuKα radiation (λ = 1.5405A°) over the scan range 4–80°. The generator voltage was 40 kV, and the generator current was 30 mA. All measurements were carried out in the continuous scan mode; the scan speed was 8° min^{-1}. The chemical structure of samples was investigated using Fourier Transform Infrared Spectroscopy (FT-IR, Shimadzu Prestige-21 Spectrophotometer) in the 4000–500 cm^{-1} range. A Witec Alpha 300 R confocal Raman spectroscope with a Nd:Yag laser excitation source(532 nm) was employed to evaluate the structural defects of the samples in the range of 1000–2000 cm^{-1} at room temperature. The surface morphology was examined by scanning electron microscopy (SEM, Hitachi-4200). The samples were sputter-coated by a thin layer of gold to be ready for scans and measurements. The sputtering process occurred at 30 mA for 30 s. The thermal analysis of the samples was executed by a Thermogravimetric analyzer (TGA, Shimadzu -50). The heating was executed under a nitrogen atmosphere; the heating rate was 10 °C min^{-1}; the temperature range was 25–600 °C. The high-resolution transmission electron microscope (HRTEM, jeol-jem2100) was done at an operating voltage of 200 kV.

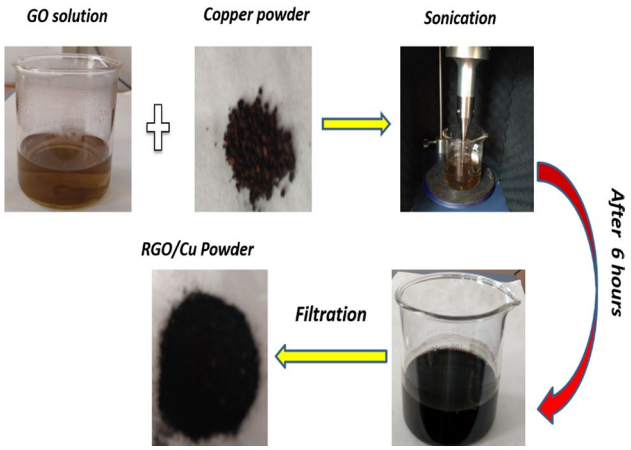

Fig. 1 Schematic representation of RGO/Cu nanocomposites synthesis

Determination of the anticancer activity of graphene oxide/copper nanocomposites (RGO/Cu) in vitro

MTT cytotoxicity assay

Initially, as represented by the procedure in Ref (Freimoser et al. 1999). MCF-7 cells (1×10^5 per well) were cultured with different RGO/Cu composite in a ratio of 1:1 (0–1600 µg/ml) in 5% CO_2 incubator for 24 h. To initiate the coloring reaction, the standard MTT solution was diluted to a final concentration of 0.5 mg MTT/ml. 300 µl of diluted MTT solution was added to each culture in a 5% CO_2 incubator for 4 h. The cells were then pelleted by centrifugation at 15.000 rpm for 5 min, and then, the media was removed. Then, 500 µl of isopropanol/HCl mixture were added, and then, tubes were well-vortexed to dissolve the formazan crystals and pelleted by centrifugation at 15.000 rpm for 5 min.

The supernatants were collected, and the absorbance was measured using a spectrophotometer (Helios, UV/Visible, UK) at 560 nm. An isopropanol/HCl mixture was used as a blank sample and subtracted from all values. The cell viability was calculated as follows:

$$\text{Viable cell (\%)} = (\text{sample absorbance} - \text{blank absorbance}/\text{control absorbance} - \text{blank absorbance}) \times 100$$

Determination of the anti-metastatic, antiproliferative, and apoptotic activities of graphene oxide/copper nanocomposites (RGO/Cu) in vitro

Quantitative PCR was applied to determine MMP 9, Bcl-2, P53, and Cathepsin D, expression. The RNeasy mini kit was used for RNA isolation and quantitative RT-PCR. The total RNA was insulated from MCF-7 cells rendering to the manufacturer's instructions. The RNA to-cDNA™ kit was used to convert RNA to cDNA. Human MMP9, Cathepsin D, Bcl-2, and P53 mRNA were quantified by qRT-PCR (Taq-Man) with specific primers and Taq-Man Fast Advanced Master Mix. All PCR reactions were executed in triplicate for each sample. The qRT-PCR data were analyzed by the Livak method (ΔΔCt), where GAPDH was used for normalization as an internal control (Livak and Schmittgen 2001).

Statistical analysis

The statistical analysis of the results was implemented by One-Way ANOVA ($P < 0.05$), Duncan's multiple ranges, and the least significant difference summary (LSD). All data analysis was carried out by SPSS software 20.0.

Results and discussion

Structural and thermal properties of RGO/Cu nanocomposites

XRD was employed to verify the reduction in GO with Cu particles and study the structural changes of GO during the reduction process.

Figure 2 shows the XRD pattern of Cu, GO, and different RGO/Cu composites. Cu shows the main diffraction peaks at ~ 43.38°, 50.50°, and 74.17° attributed to (111), (200), and (220) planes, respectively, which are very similar to those of the face-centered cubic Cu phase (JCPDS No. 04-0836) (Theivasanthi and Alagar 2010). The weak peak at 36.49° assigned to the (111) crystal plane due to partially surface oxidation of Cu in the air (JCPDS No. 01-077-0199) (Yang et al. 2014; Li et al. 2016). GO pattern shows characteristic diffraction peaks at 9.6°due to (001) reflection plane of the stacked GO sheets.

In RGO/Cu15 pattern, the GO diffraction peak is seen to become broader and shifted to 12.2° with d-value = 7.2 Å followed by a wide broad peak at 24.2°, indicating a weak reduction degree of RGO/Cu15 (Hong et al. 2016). The peak observed at 26.6° attributed to the (002) plane of highly ordered reduced graphene oxide (Saleem et al. 2014). Also, very small diffraction peaks at 36.4° and 43.4° were observed, indicating Cu particles combined with RGO (Fakhri et al. 2014). Also, very small peaks at 40.3° and 42.1° suggest the formation of additional CuO phases during reduction consistent with standard card (JCPDS Card No. 48–1548) (Zhao et al. 2013). The RGO/Cu30 and the RGO/Cu50 patterns show only RGO broad peak at ~ 24.2°, which indicates the efficient reduction in GO with rising Cu percentage. Furthermore, the Cu and CuO peaks became more predominant.

FTIR gives important information about functional groups held on different samples and helps verify the GO reduction process. FTIR spectra of Cu, GO, and different RGO/Cu nanocomposites are shown in Fig. 3. The Cu spectrum shows small bands at ~ 3334 cm^{-1}due to O–H vibration while bands at 1235–1034 cm^{-1} due to C-O groups, which reveals the oxidation of Cu surface as confirmed previously by XRD (Arun et al. 2015; Naikoo et al. 2014). Furthermore, the strong band at 525 cm^{-1} corresponding to Cu–O vibrations reveals an oxidized surface of Cu particles consistent with XRD data (Liu et al. 2013). The FTIR spectra

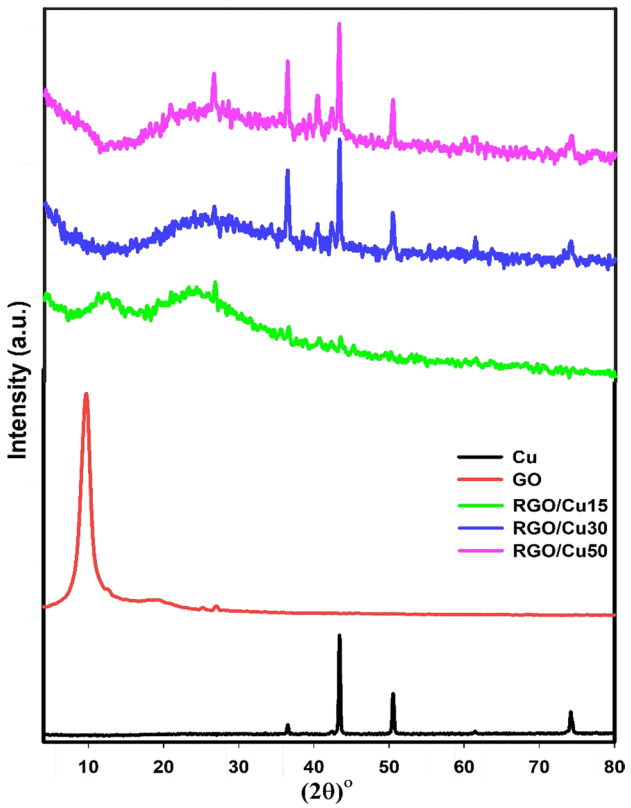

Fig. 2 XRD pattern of Cu, GO, and different RGO/Cu nanocomposites

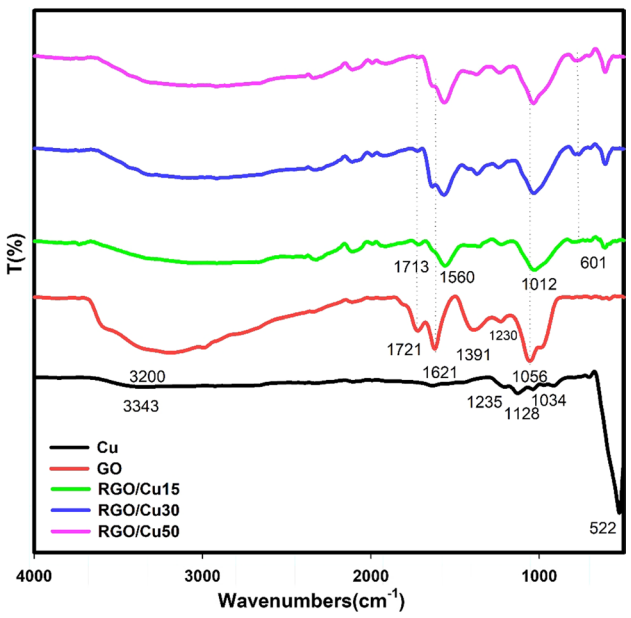

Fig. 3 FTIR Spectra of Cu, GO, and different RGO/Cu nanocomposites

of GO show abundant oxygen functional groups where a strong broad band around 3200 cm^{-1} owing to O–H stretching vibrations detected. Also, the stretching vibrations of C=O at 1721 cm^{-1}, C–OH at 1391 cm^{-1}, C–O at 1230 and 1056 cm^{-1} were observed. The vibrations of unoxidized graphitic domains C=C at 1621 cm^{-1} were detected (Meng et al. 2010; Wojtoniszak et al. 2012). Compared to GO, the decreased intensity of oxygen functional bands in RGO/Cu15 confirms the successful reduction in GO by Cu particles (Choi et al. 2010). As well as, a new band detected at 609 cm^{-1} attributed to Cu–O phase formation consistent with other reports (Zhao et al. 2012; Nagajyothi et al. 2017). FTIR spectrum of RGO/Cu30 shows further decreasing the intensity of C=O at 1713 cm^{-1} as well as the C=C vibration at 1635 cm^{-1} became more obvious. This suggests a higher reduction degree of RGO/GO30 compared to RGO/GO15 which is consistent with XRD results. Besides, the increasing intensity of C–OH and the Cu–O band observed suggest more Cu–O phase formed due to the higher incorporation ratio of Cu into GO. The very similar FTIR spectra of RGO/Cu30 and RGO/Cu50 suggest a convergent reduction degree.

Raman spectroscopy is a well-recognized technique to examine the structure of carbon-based materials. Figure 4 shows the Raman spectrum of GO and RGO/Cu nanocomposites. Two characteristic bands were noticed in the GO spectrum, the D band at 1335 cm^{-1} and the G at 1580 cm^{-1}. The G band represents the crystalline graphite with E_{2g} zone center mode, whereas the D band designates the broken symmetry at edges or defects in the sample (Mohan et al. 2015). Also, all RGO/Cu samples have more broadening D and G bands indicate their higher disorder (Mohan et al. 2015).

The percentage of D and G bands intensities (ID/IG) of the graphitic materials is often used as a meter of their degree of structural defects (Tuinstra and Koenig 1970). According to Fig. 4, the ID/IG for all RGO/Cu nanocomposites is higher than GO, indicating their higher defect level

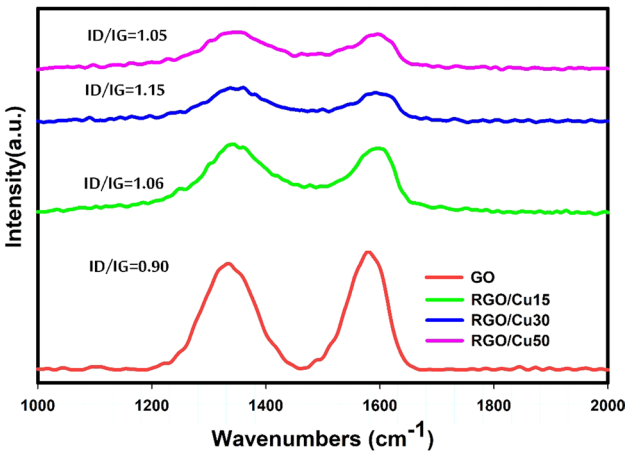

Fig. 4 Raman Spectra for GO, and different RGO/Cu nanocomposite

and successful reduction, consistent with other reports (Song et al. 2013). Also, RGO/Cu30 has the highest value of ID/IG suggests it has the most abundant and smallest graphitic domains compared to other samples (Xu et al. 2015).

The SEM images of Cu, GO, and different RGO/Cu nanocomposites are shown in Fig. 5. The Cu particles show an irregular shape, while GO shows a smooth structure with slightly corrugated sheets. In contrast, RGO/Cu15 showed restacked sheets with aggregated and fracture structures owing to the self-assembly via Van der Waals' forces through the reduction (Hou et al. 2016). Further restacking sheets and aggregation were observed by further increasing the copper ratio. This confirms a complete reduction in GO by adding 30 and 50% of Cu particles which consistent with XRD and FTIR findings (Viswanathan and Shetty 2018).

Figure 6 shows HRTEM images of Cu, GO, and all RGO/Cu nanocomposites. Most Cu particles are polyhedral with an average size of ~ 107 nm. A few Cu nanorods of range ~ 49 nm were also observed. Most Cu particles show inhomogeneous contrast regions within one particle, demonstrating their polycrystalline nature (Cheng and Walker 2010). Also, the HRTEM image shows GO transparent and soft sheets with few wrinkles that have been exfoliated into several layers, which is consistent with the literature (Hsieh et al. 2011). HRTEM images of RGO/Cu nanocomposites show crumpled morphology and folded appearance of RGO sheets which confirm the reduction process in agreement with the literature (Hou et al. 2016). Besides, Cu nanoparticles irregularly decorated RGO sheets with some aggregation occurred with increasing its concentration. Also, Cu particle size decreased greatly upon incorporation with GO which demonstrates the effect of sonication on Cu particles as reported previously (Pradhan et al. 2016; Lee et al. 2017).

Figure 7 shows the TGA curves of GO and different RGO/Cu nanocomposites. The TGA curve of GO shows three distinct temperature spans. The first spans from ambient temperature to ~ 150 °C; the weight loss is due to loosely bonded or adsorbed water and gas molecules; the second is 150–250 °C created by the decay of labile oxygen groups (such as carboxylic, anhydride, or lactone groups). The third temperature span is 250–600 °C, due to more thermally stable oxygen functionalities (Jeong et al. 2009). TGA curves of different RGO/Cu nanocomposites show increased thermal stability of GO by the continuous increment of Cu ratio, which is indirect proof of the GO successful reduction (Ganguly et al. 2011).

Cell inhibition behavior of RGO/Cu nanocomposites using MTT

It was displayed due to its intrinsic size- and shape-dependent optical characteristics, unique physicochemical behavior,

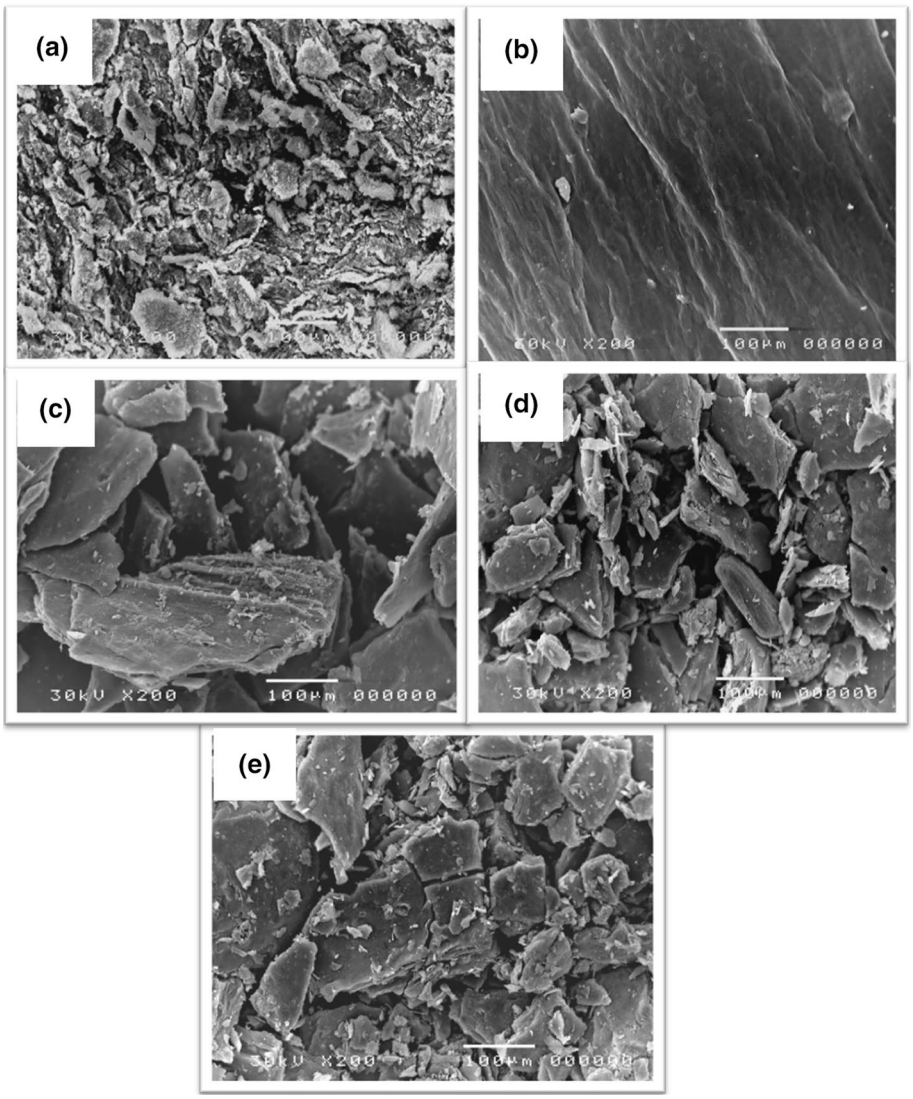

Fig. 5 SEM images for Cu (**a**), GO (**b**), RGO/Cu15 (**c**), RGO/Cu30 (**d**), and RGO/Cu50 (**e**)

very large surface to volume ratio, and flexible surface features, and graphene oxide has been regarded as an intriguing nanomaterial for cancer treatment (Shanbhag and Prasad 2016)

A comprehensive investigation was carried out to assess the cytotoxicity of RGO/Cux nanocomposites toward MCF-7 cells and to determine the likelihood of cell.

Figure 8 shows the results of the cytotoxic effect of RGO/Cu15, RGO/Cu30, and RGO/Cu50 against MCF-7 and the obtained data shown in Table 1. The cell viability was observed in MCF-7 cells incubated with different concentrations of RGO/Cu nanocomposites using MTT test. Viable MCF-7 cells incubated in RPMI complete media were considered as a positive control (100% viability). The highest inhibitory concentration for RGO/Cu15 is 1600 µg/ml which displayed 84.2% MCF-7 cells inhibition after 24 h of incubation, while the lowest inhibitory concentration is 25 µg/ml. Also, the highest inhibition values of MCF-7 cells treated with 1600 µg/ml from RGO/Cu30 and RGO/Cu50 are 94.2% and 88.8%, respectively. Compared to other complexes, RGO/Cu30 unveiled the maximum inhibition at different concentrations (Yuan and Gurunathan 2017). The IC50 value shows how much of a nanocomposite (RGO/Cux nanocomposites) is required to inhibit in vitro cell viability of cancer cell line (MCF-7) by 50%, calculated by GraphPad Prism 7 program (Hoetelmans 2011). RGO/Cu30 had a more noticeable inhibitory effect on the cell viability than other RGO/Cu nanocomposite with minimum IC50 75.40 µg/ml. The results suggested RGO/Cu30 perform further experiments. These findings revealed the link between notable cell viability loss and reactive oxygen species (ROS), which illustrated the substantial malignant cell/tissue damage caused only by cell necrosis/apoptosis (Adil et al. 2021).

According to Vallabani et al., the cytotoxicity of graphene oxide has also been demonstrated in HBI.F3 human

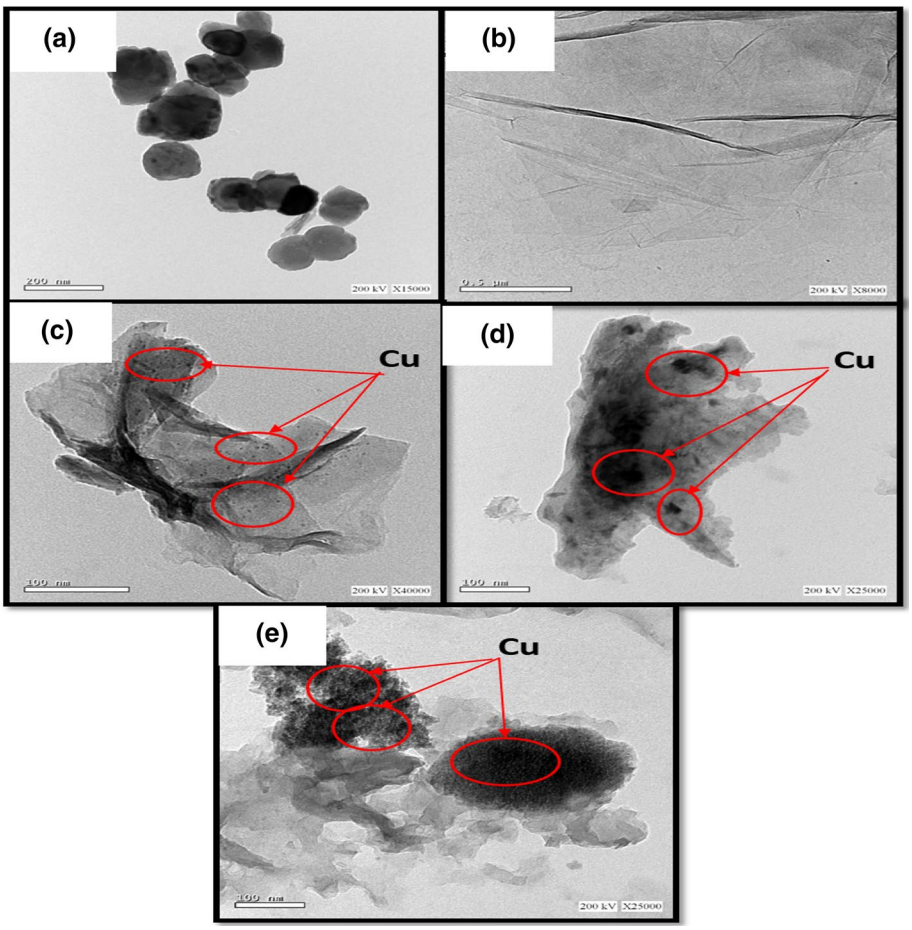

Fig. 6 HRTEM images of Cu (**a**), GO (**b**), RGO/Cu15 (**c**), RGO/Cu30 (**d**), and RGO/Cu50 (**e**)

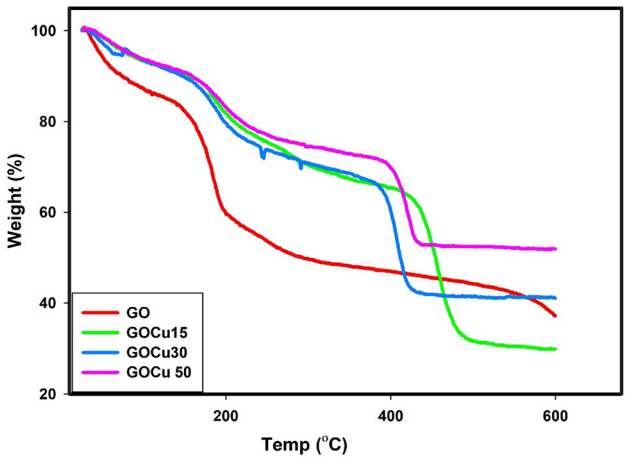

Fig. 7 TGA curves for Cu, GO, and different RGO/Cu nanocomposites

neuronic cells and BEAS-2B human lung cells, with cell viability being reduced at doses of 10–100 g/mL. Furthermore, both early and late apoptosis of cells was increased (Vallabani et al. 2011).

Adil et al. revealed that in all examined cancer cell lines, lung (A549), liver (HepG2), and breast (MCF-7), highly reduced graphene oxide (HRG) caused a concentration-dependent decrease in cell viability.

The RGO/Cu30-dependent changes of relative gene expression of Cathepsin D, and MMP9 produced by these cells as determined by RT-PCR as shown in Table 2. The RGO/Cu30 decreased the gene expression of Cathepsin D, and MMP9 in MCF-7 cells.

Figure 9 represents the RGO/Cu30-induced apoptosis through significant induction of gene expression of P53 and significantly inhibits anti-apoptotic Bcl-2 gene expression by 2.41 and − 1.73 as associated with gene expression in untreated MCF-7 cells, respectively. It means (RGO/Cu30 + MCF-7) P53 gene expression = (2.41 fold) MCF-7 p53 gene expression and (RGO/Cu30 + MCF-7) Bcl-2 gene expression = (− 1.73 fold) MCF-7 p53 gene expression. Anti-Metastatic activity induces apoptosis against MCF-7 by trigging reactive oxygen species (ROS). The free radicals were induced by lipid peroxidation, which is the main reason for oxidative stress, and antioxidant depletion in MCF-7 cells was induced by RGO/Cu30. Cathepsin and MMP-9 were significantly inhibited by − 4.1 and − 2.24,

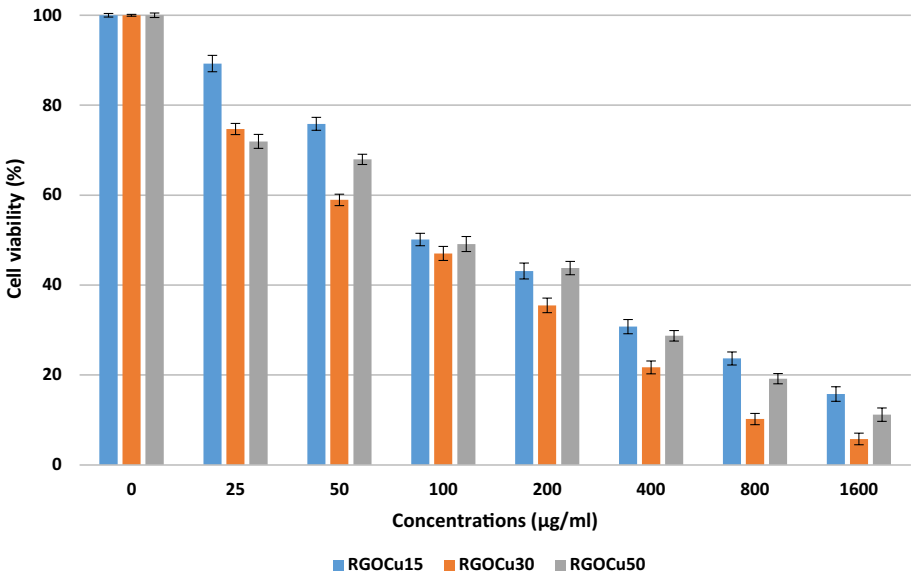

Fig. 8 Cell viability in EAC cells incubated with different RGO/Cu nanocomposites

Table 1 Cell viability and inhibition in MCF-7 cells incubated for 24 h with different RGO/Cu nanocomposites by MTT (3-(4,5-dimethylthiazol-2yl)-2,5-diphenyltetrazolium bromide) assay

	Cell viability (%) Mean ± SD			Cell inhibition (%) mean		
Concentration (µg/ml)	RGO/Cu15	RGO/Cu30	RGO/Cu50	RGO/Cu15	RGO/Cu30	RGO/Cu50
0	100.0 ± 0.4	100.0 ± 0.2	100.0 ± 0.5	0.0 ± 0.4	0.0 ± 0.2	0.0 ± 0.5
25	89.3 ± 1.82	74.7 ± 1.24	72.0 ± 1.55	10.7 ± 1.82	25.3 ± 1.24	28 ± 1.55
50	75.9 ± 1.44	58.9 ± 1.27	68.0 ± 1.14	24.1 ± 1.44	41.1 ± 1.27	32 ± 1.14
100	50.1 ± 1.38	47.0 ± 1.56	49.1 ± 1.67	49.9 ± 1.38	53 ± 1.56	50.9 ± 1.67
200	43.1 ± 1.77	35.5 ± 1.62	43.8 ± 1.48	56.9 ± 1.77	64.5 ± 1.62	56.2 ± 1.48
400	30.8 ± 1.58	21.7 ± 1.43	28.7 ± 1.17	69.2 ± 1.58	78.3 ± 1.43	71.3 ± 1.17
800	23.7 ± 1.45	10.2 ± 1.25	19.2 ± 1.14	76.3 ± 1.45	89.8 ± 1.25	80.8 ± 1.14
1600	15.8 ± 1.62	5.8 ± 1.29	11.2 ± 1.19	84.2 ± 1.62	94.2 ± 1.29	88.8 ± 1.19
IC50 (µg/ml)	**84.93**	**75.40**	**82.83**			
R^2	**0.8437**	**0.7263**	**0.7378**			

IC50: Half maximal inhibitory concentration. R^2 (R Squared): The value R^2 for the results of nonlinear and multiple regression quantifies goodness of the best-fit curve. It compares the fit of your model to the fit of a horizontal line through the mean of all Y values

Table 2 The gene expression of P53, Bcl-2, Cathepsin D, and MMP9 as ΔCT and fold gene expression in MCF-7 and post 24 h incubation with RGO/Cu30

Genes	MCF-7 (ΔCT)	MCF-7 + RGOCu30 (ΔCT)	Fold change
P53	2.13 ± 0.11	0.87 ± 0.11	2.41 ± 0.34
Bcl-2	− 0.99 ± 0.14	0.22 ± 0.1	− 1.73 ± 0.35
Cathepsin	− 1.3 ± 0.21	0.71 ± 0.35	− 4.1 ± 0.83
MMP9	− 0.98 ± 0.2	0.18 ± 0.1	− 2.24 ± 0.11

respectively, compared to gene expression in untreated MCF-7 cells. It means (RGO/Cu30 + MCF-7) Cathepsin gene expression = (− 4.1fold) MCF-7 Cathepsin gene expression and (RGO/Cu30 + MCF-7) MMP-9 gene

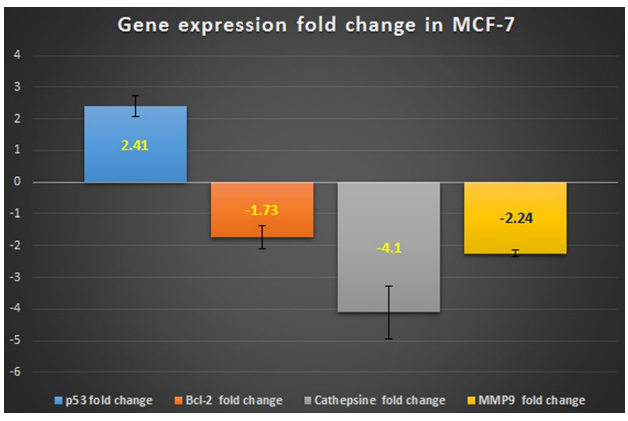

Fig. 9 The effect of RGO/Cu30 composite on gene expression of P53, Bcl-2, Cathepsin D, and MMP9 as fold gene expression in MCF-7

expression = (− 2.24 fold) MCF-7 MMP-9 gene expression (Yuan and Gurunathan 2017).

The importance of ROS in cytotoxicity has been documented in several studies. One of the toxicological processes proposed for many graphene-based nanomaterials is reactive oxygen species (ROS) (Shaheen et al. 2018). Cell-belting down influences, such as apoptosis or necrosis, are influenced by ROS growth (Ajdari et al. 2016). Furthermore, ROS focuses on mitochondria, causing cellular death by vascular blockage (Wu and Yotnda 2011). The results clearly demonstrated that the GO–ZnO nanocomposite has a substantial effect on ROS production at various dosages (10–100 µg/mL).

These findings indicated that GO-ZnO released ROS and inhibited MCF-7 cell growth by promoting oxidative stress, which might be useful for creating effective graphene-associated derivatives, especially for biomedical applications (Xu et al. 2015).

It was presented that lung (A549), liver (HepG2), and breast (MCF-7) were treated with highly reduced graphene oxide (HRG), which resulted in a greater ROS concentration, resulting in cell damage and apoptosis (Adil et al. 2021).

The ROS was overproduced by the cellular cell inflammation, proliferation, and apoptosis, and further cell death has been reported via ROS elevation (Redza-Dutordoir and Averill-Bates 2016). This finding suggested that the cytotoxic effect exerted by RGO/Cu30 is associated with ROS generation. Apoptosis was induced by RGO/Cu30 in MCF-7 cells by induction of the gene expression of P53, and p53, Bax/bcl-2, and caspase pathways (Jabir et al. 2019). Furthermore, we found pro-apoptotic members of the Bcl-2 family, such as Bax induces permeability of the outside mitochondrial membrane, which releases soluble proteins into the cytosol, where they promote caspase activation (Kale et al. 2018).

Caspase-3 and caspase-9 in cervical cancer cells were activated by RGO lead to apoptosis. Furthermore, the cytotoxic effect exerted by RGO/Cu30 is associated with decreasing the proliferation in MCF-7 cell line where anti-apoptotic Bcl-2 family, Bcl-2 gene expression was decreased after 24 h incubation with RGO/Cu30 (Jabir et al. 2019). Furthermore, Cathepsin D and MMP9 gene expressions were decreased by RGO/Cu30 24 h incubation with MCF-7 cell line.

Ganesan et al. (Ganesan et al. 2020) reported that CuO-GO nanocomposites medication has improved antitumor efficacy via various mechanisms. GO served as a tumor inhibitor as well as a vehicle for medication delivery. The cytotoxic action of the caspase cascade of apoptosis, DNA damage, and mitochondrial dysfunction is mediated by the generation of reactive oxygen species (ROS) by CuO-GO nanocomposites.

Table 3 The correlation (r) between the gene fold expression of P53, Bcl-2, Cathepsin, and MMP9 in MCF-7 $P < 0.01$

Fold change	P53	Bcl-2	Cathepsin
Bcl-2	− 0.880*		
Cathepsin	− 0.944*	0.935*	
MMP9	− 0.928*	0.896*	0.973*

*Correlation is significant at 0.01

Table 3 represents the negative correlation among p53, Bcl-2, Cathepsin D, and MMP-9 by − 0.880, − 0.944, and − 0.928, respectively. Furthermore, a positive correlation has been reported among Bcl-2, Cathepsin D, and MMP-9 via 0.935 and 0.896, respectively, as well as between Cathepsin and MMP-9 by 0.973.

The RGO suppressed MCF-7 cell growth, resulting in programmed cell death, via activating the mitochondrial-mediated signaling system, which included the NF-kB signaling pathway, suppression of NF-κB translocation, mitochondrial membrane potential (MMP), induction reactive oxygen species (ROS) production, and down-regulate bcl-2 and up-regulate Bax gene expressions (Alsaedi et al. 2019).

According to Ahamed et al. (Ahamed et al. 2021), the anticancer activity of SnO_2-ZnO/RGO nanocomposites was substantially greater than that of SnO_2-ZnO NPs and ZnO NPs in MCF-7 cancer cells. Through activation of the caspase-3 gene and reduction in mitochondrial membrane potential MMP-9, the SnO_2-ZnO/RGO NCs caused an apoptotic response. SnO_2-ZnO/RGO NCs destroy cancer cells via an oxidative stress route, according to a mechanistic analysis (Ahamed et al. 2021).

Cathepsin D and MMP9 in breast cancer were involved in cell metastasis and invasion via hydrolysis of collagens, fibronectin, and proteoglycans by their lysosomal aspartic protease activity (Oskarsson 2013). Cathepsin D and MMP9 increase the cell growth and tumorigenesis of MCF-7 both in vitro and in vivo. The tumor metastasis was induced in ER-negative breast cancer cells by inhibiting c-Myb by collagenase activity of Cathepsin D and MMP9 (Knopfová et al. 2012).

Cathepsin D and MMP9 in breast cancer cells were reduced by RGO/Cu30. In MCF7 cells, MMP9 has upregulated (Fujita et al. 2018) and collagen IV. Growth factors released and extracellular matrix degradation was enhanced by Cathepsin D via its proteolytic activity to facilitate tumor invasion (Tabish et al. 2019).

Tanveer et al. revealed that GO adsorb these pro-tumorigenic enzymes (Cathepsin D and Cathepsin L) as part of tailored anti-metastatic therapy. CathD/L was adsorbed onto

the surface of GO via its cationic and hydrophilic residues, according to the results of CathD/L binding to GO.

Conclusion

Different series of RGO/Cu nanocomposites (RGO/Cu15, RGO/Cu30, and RGO/Cu50) were successfully synthesized sonochemically. The XRD shows that GO was partially reduced in RGO/Cu15 while increasing the reduction degree observed as the Cu ratio increased in nanocomposites. Also, FTIR confirms the successful reduction in GO by Cu particles and the formation of new CuO phases. From Raman spectroscopy, the higher ID/IG of RGO/Cu nanocomposites than GO designates their higher defect level and effective reduction. The RGO/Cu30 nanocomposite had the highest value of ID/IG, which recommends its greatest and smallest graphitic domains. The SEM images showed restacked and agglomerated morphology of GO sheets upon the addition of Cu particles which confirms the effective reduction by Cu particles. HRTEM images showed that Cu nanoparticles irregularly decorated RGO sheets with some aggregation occurred with increasing its concentration. The thermal stability of GO was increased with the increment of Cu content on RGO/Cu nanocomposites. The cell viability was observed in MCF-7 cells incubated with different concentrations of RGO/Cu nanocomposites using MTT test. A greater inhibitory concentration value for RGO/Cu15 at 1600 µg/ml exhibited 84.2% after 24 h of incubation. In contrast, the inhibitory value was 94.2 and 88.8 for RGO/Cu30 and RGO/Cu50, respectively. So, RGO/Cu30 is selected for further work. Generally, the present study provides proof of RGO/Cu30 to apply cytotoxic anticancer and anti-metastatic activities. Cathepsin D and MMP9 gene expressions were inhibited by RGO/Cu30 lead to the inhibition of MCF-7 breast cancer metastasis. The apoptotic and antiproliferative activities of RGO/Cu30 are associated with increased P53 and decreased Bcl-2 gene expressions.

Acknowledgements The authors would like to express their gratitude and appreciation to National Centre for Radiation Research and Technology (NCRRT), Egyptian Atomic Energy Authority, Cairo, Egypt for supporting and providing materials for this work.

Declarations

Conflict of interest The authors declare no conflict of interest.

Consent to participate On the behalf on authors, the corresponding author confirms that all authors mentioned in the manuscript have agreed for authorship.

Consent for publication On the behalf on authors, the corresponding author confirms that all authors mentioned in the manuscript have given consent for submission and subsequent publication of the manuscript.

References

Adil SF, Shaik MR, Nasr FA, Alqahtani AS, Ahmed MZ, Qamar W et al (2021) Enhanced apoptosis by functionalized highly reduced graphene oxide and gold nanocomposites in MCF-7 breast cancer cells. ACS Omega 6:15147–15155

Ahamed M, Akhtar MJ, Khan MM, Alhadlaq HA (2021) SnO_2-Doped ZnO/reduced graphene oxide nanocomposites: synthesis, characterization, and improved anticancer activity via oxidative stress pathway. Int J Nanomed 16:89

Ahmed R, Ibrahiem A, El-Bayoumi A, Atta M (2021) Structural, mechanical, and dielectric properties of polyvinylchloride/graphene nano platelets composites. Int J Polym Anal Charact 26:68–83

Ai J, Xu W, Zhang R, Su K, Hu L, Cheng L, Ouyang X, Li W (2019) Facile synthesis of magnetic reduced graphene oxide-$ZnFe_2O_4$ composites with enhanced visible-light photocatalytic activity. In: IOP Conference Series: Materials Sci & Engineering. IOP Publishing: p. 012155

Ajdari Z, Rahman H, Shameli K, Abdullah R, Abd Ghani M, Yeap S et al (2016) Novel gold nanoparticles reduced by Sargassum glaucescens: preparation, characterization and anticancer activ. Molecules 21:123

Alsaedi II, Taqi ZJ, Hussien AMA, Sulaiman GM, Jabir MS (2019) Graphene nanoparticles induces apoptosis in MCF-7 cells through mitochondrial damage and NF-KB pathway. Mate Res Express 6:095413

Arun K, Batra A, Krishna A, Bhat K, Aggarwal M, Francis PJ (2015) Surfactant free hydrothermal synthesis of copper oxide nanoparticles. Amer J Mater Sci 5:36–38

Atta M, Taha EO, Abdelreheem A (2021a) Nitrogen plasma effect on the structural, thermal, and dynamic mechanical properties of PVA/starch/graphene oxide nanocomposite. Appl Phys A 127:1–10

Atta MM, Abdel Maksoud MIA, Sallam OI, Awed AS (2021b) Gamma irradiation synthesis of wearable supercapacitor based on reduced graphene oxide/cotton yarn electrode. J Mater Sci Mater Elect 32:3688–3698

Bitounis D, Ali-Boucetta H, Hong BH, Min DH, Kostarelos K (2013) Prospects and challenges of graphene in biomedical applications. Adv Mater 25:2258–2268

Burrows CJ, Muller JG (1998) Oxidative nucleobase modifications leading to strand scission. Chem Rev 98:1109–1152

Cheng G, Walker AH (2010) Transmission electron microscopy characterization of colloidal copper nanoparticles and their chemical reactivity. Anal Bioanaly Chem 396:1057–1069

Choi EY, Han TH, Hong J, Kim JE, Lee SH, Kim HW, Kim SO (2010) Noncovalent functionalization of graphene with end-functional polymers. J Mater Chem 20:1907–1912

Dobrovolný K, Ulbrich P, Švecová M, Rimpelova S, Malinčík J, Kohout M et al (2017) Copper nanoparticles in glycerol-polyvinyl alcohol matrix: in situ preparation, stabilisation and antimicrobial activity. J Alloy Comp 697:147–155

Fakhri P, Jaleh B, Nasrollahzadeh M (2014) Synthesis and characterization of copper nanoparticles supported on reduced graphene oxide as a highly active and recyclable catalyst for the synthesis of formamides and primary amines. J Mol Catal A Chem 383:17–22

Freimoser FM, Jakob CA, Aebi M, Tuor U (1999) The MTT [3-(4, 5-dimethylthiazol-2-yl)-2, 5-diphenyltetrazolium bromide] assay is a fast and reliable method for colorimetric determination of fungal cell densities. Appl Environ Microbiol 65:3727–3729

Fujita K, Take S, Tani R, Maru J, Obara S, Endoh S (2018) Assessment of cytotoxicity and mutagenicity of exfoliated graphene. Toxicol Vitr 52:195–202

Ganesan K, Jothi VK, Natarajan A, Rajaram A, Ravichandran S, Ramalingam S (2020) Green synthesis of Copper oxide nanoparticles decorated with graphene oxide for anticancer activity and catalytic applications. Arab J Chem 13:6802–6814

Ganguly A, Sharma S, Papakonstantinou P, Hamilton J (2011) Probing the thermal deoxygenation of graphene oxide using high-resolution in situ X-ray-based spectroscopies. J Phys Chem C 115:17009–17019

Goldsmith BR, Locascio L, Gao Y, Lerner M, Walker A, Lerner J, Kyaw J, Shue A, Afsahi S, Pan D (2019) Digital biosensing by foundry-fabricated graphene sensors. Sci Rep 9:1–10

Hoetelmans R (2011) PK-PD relationships for antiretroviral drugs. FDA, Amsterdam, The Netherlands

Hong Y, Hua H, Huan Y, Qiong X, Lin A, Ping H, Lin G, Chenab W (2016) Partially reduced graphene oxide as highly efficient DNA nanoprobe. Biosen Bioelect 80:140–145

Hou D, Liu Q, Cheng H, Li K, Wang D, Zhang H (2016) Chrysanthemum extract assisted green reduction of graphene oxide. Mater Chem Phys 183:76–82

Hsieh CT, Hsu SM, Lin JY, Teng H (2011) Electrochemical capacitors based on graphene oxide sheets using different aqueous electrolytes. J Phys Chem C 115:12367–12374

Hu Z, Huang Y, Sun S, Guan W, Yao Y, Tang P, Li C (2012) Visible light driven photodynamic anticancer activity of graphene oxide/TiO_2 hybrid. Carbon 50:994–1004

Huma R, Mahmud T, Munir R, Munir SJ, Iftikhar K (2019) Cytotoxicity and molecular docking studies of a novel enaminone and its cadmium (II) complex. Pak J Zool. https://doi.org/10.17582/journal.pjz/2019.51.2.697.702

Hunge Y, Yadav A, Liu S, Mathe V (2019) Sonochemical synthesis of CZTS photocatalyst for photocatalytic degradation of phthalic acid. Ultrason Sonochem 56:284–289

Jabir MS, Taha AA, Sahib UI, Taqi ZJ, Al-Shammari AM, Salman AS (2019) Novel of nano delivery system for Linalool loaded on gold nanoparticles conjugated with Calnn peptide for application in drug uptake and induction of cell death on breast cancer cell line. Mater Sci Eng C 94:949–964

Jain S, Hirst D, O'sullivan J (2012) Gold nanoparticles as novel agents for cancer therapy. Br J Radiol 85:101–113

Jakus AE, Secor EB, Rutz AL, Jordan SW, Hersam MC, Shah RN (2015) Three-dimensional printing of high-content graphene scaffolds for electronic and biomedical applications. ACS Nano 9:4636–4648

Jeong H, Jin M, So K, Lim S, Lee Y (2009) Tailoring the characteristics of graphite oxides by different oxidation times. J Phys D Appl Phys 42:065418

Jose GP, Santra S, Mandal SK, Sengupta TK (2011) Singlet oxygen mediated DNA degradation by copper nanoparticles: potential towards cytotoxic effect on cancer cells. J Nanobiotechnol 9:9

Kale J, Osterlund EJ, Andrews DW (2018) BCL-2 family proteins: changing partners in the dance towards death. Cell Death Diff 25:65–80

Katikireddi RS, Setty RS (2013) The incidence of common cancers in south Indian region –a hospital based cross sectional study-research article. Int J Curr Res Rev 5:37

Knopfová L, Beneš P, Pekarčíková L, Hermanová M, Masařík M, Pernicová Z, Souček K, Šmarda J (2012) c-Myb regulates matrix metalloproteinases 1/9, and cathepsin D: implications for matrix-dependent breast cancer cell invasion and metastasis. Mol Cancer 11:1–15

Laha D, Pramanik A, Maity J, Mukherjee A, Pramanik P, Laskar A, Karmakar P (2014) Interplay between autophagy and apoptosis mediated by copper oxide nanoparticles in human breast cancer cells MCF7. Biochim Et Biophys Acta (BBA)-Gen Sub 1840:1–9

Lee S, Jeong H, Noh Y, Hyun SK, Lee D, Jin C (2017) Preparation of Cu nanoparticles with controlled particle size and distribution via reaction temperature and sonication. Surf Interface Anal 49:405–409

Li J, Zhang Z, Ji Y, Jin Z, Zou S, Zhong Z, Su F (2016) One-dimensional Cu-based catalysts with layered Cu–Cu 2 O-CuO walls for the Rochow reaction. Nano Res 9:1377–1392

Liu Y, Ying Y, Mao Y, Gu L, Wang Y, Peng X (2013) CuO nanosheets/rGO hybrid lamellar films with enhanced capacitance. Nanoscale 5:9134–9140

Livak KJ, Schmittgen TD (2001) Analysis of relative gene expression data using real-time quantitative PCR and the 2− ΔΔCT method. Methods 25:402–408

Lu X (2019) Reduced graphene oxide biosensors for prostate cancer biomarker detection, PhD Thesis, Justus-Liebig-Universität Gießen

Marcano DC, Kosynkin DV, Berlin JM, Sinitskii A, Sun Z, Slesarev A, Alemany LB, Lu W, Tour JM (2010) Improved synthesis of graphene oxide. ACS Nano 4:4806–4814

McAllister MJ, Li JL, Adamson DH, Schniepp HC, Abdala AA, Liu J, Herrera-Alonso M, Milius DL, Car R, Prud'homme RK (2007) Single sheet functionalized graphene by oxidation and thermal expansion of graphite. Chem Mater 19:4396–4404

Meng X, Geng D, Liu J, Banis MN, Zhang Y, Li R, Sun X (2010) Non-aqueous approach to synthesize amorphous/crystalline metal oxide-graphene nanosheet hybrid composites. J Phys Chem C 114:18330–18337

Metcalfe C, Thomas JA (2003) Kinetically inert transition metal complexes that reversibly bind to DNA. Chem Soc Rev 32:215–224

Mohan VB, Brown R, Jayaraman K, Bhattacharyy D (2015) Characterisation of reduced graphene oxide: effects of reduction variables on electrical conductivity. Mater Sci Eng B 193:49–50

More MP, Chitalkar RV, Bhadane MS, Dhole SD, Patil AG, Patil PO, Deshmukh PK (2019) Development of graphene-drug nanoparticle based supramolecular self assembled pH sensitive hydrogel as potential carrier for targeting MDR tuberculosis. Mater Technol 34:324–335

Moussa S, Atkinson G, SamyEl-Shall M, Shehata A, AbouZeid KM, Mohamed MB (2011) Laser assisted photocatalytic reduction of metal ions by graphene oxide. J Mater Chem 21:9608–9619

Nagajyothi PC, Muthuraman P, Sreekanth TVM, Hwan D, Shima J (2017) Green synthesis: in-vitro anticancer activity of copper oxide nanoparticles against human cervical carcinoma cells. Arab J Chem 10:215–225

Naikoo GA, Dar RA, Khan F (2014) Hierarchically macro/mesostructured porous copper oxide: facile synthesis, characterization, catalytic performance and electrochemical study of mesoporous copper oxide monoliths. J Mater Chem A 2:11792–11798

Novoselov KS, Geim AK, Morozov S, Jiang D, Katsnelson MI, Grigorieva I, Dubonos S, Firsov AA (2005) Two-dimensional gas of massless Dirac fermions in graphene. Nature 438:197

Oskarsson T (2013) Extracellular matrix components in breast cancer progression and metastasis. Breast 22:S66–S72

Pei S, Cheng HM (2012) The reduction of graphene oxide. Carbon 50:3210–3228

Pinto AM, Goncalves IC, Magalhaes FD (2013) Graphene-based materials biocompatibility: a review. Colloids Surf B Biointerf 111:188–202

Pradhan S, Hedberg J, Blomberg E, Wold S, Wallinder IO (2016) Effect of sonication on particle dispersion, administered dose and metal release of non-functionalized, non-inert metal nanoparticles. J Nanoparticle Res 18:1–14

Rahman M, Kazmi I, Beg S, Hafeez A, Afzal M, Kumar V, Anwar F, Ahmad FJ (2019) Functionalized graphene-based nanomaterials for drug delivery and biomedical applications in cancer chemotherapy. In: Nanoparticles in pharmacotherapy Elsevier, pp. 429–460

Redza-Dutordoir M, Averill-Bates DA (2016) Activation of apoptosis signalling pathways by reactive oxygen species. Biochim Et Biophys Acta (BBA) Molec Cell Res 1863:2977–2992

Saleem H, Haneef M, AbbasI HY (2014) Synthesis route of reduced graphene oxide via thermal reduction of chemically exfoliated graphene oxide. Mater Chem Phys 204:1–7

Santini C, Pellei M, Gandin V, Porchia M, Tisato F, Marzano C (2013) Advances in copper complexes as anticancer agents. Chem Rev 114:815–862

Schedin F, Geim A, Morozov S, Hill E, Blake P, Katsnelson M, Novoselov K (2007) Detection of individual gas molecules adsorbed on graphene. Nature Mater 6:652

Shadjou N, Hasanzadeh M, Khalilzadeh B (2018) Graphene based scaffolds on bone tissue engineering. Bioengineered 9:38–47

Shaheen F, Aziz MH, Fatima M, Khan MA, Ahmed F, Ahmad R et al (2018) In Vitro cytotoxicity and morphological assessments of GO-ZnO against the MCF-7 cells: determination of singlet oxygen by chemical trapping. Nanomater 8:539

Shanbhag VKL, Prasad K (2016) Graphene based sensors in the detection of glucose in saliva–a promising emerging modality to diagnose diabetes mellitus. Anal Methods 8:6255–6259

Singh SK, Singh MK, Nayak MK, Kumari S, Grácio JJ, Dash D (2011) Size distribution analysis and physical/fluorescence characterization of graphene oxide sheets by flow cytometry. Carbon 49:684–692

Song J, Xu L, Zhou C, Xing R, Dai Q, Liu D, Song H (2013) Synthesis of graphene oxide based CuO nanoparticles composite electrode for highly enhanced nonenzymatic glucose detection. ACS Appl Mater Interface 5:12928–19934

Sorenson J (1992) Use of essential metalloelement complexes or chelates in biological studies. Free Radiac Biol Med 13:593

Stankovich S, Dikin DA, Dommett GH, Kohlhaas KM, Zimney EJ, Stach EA, Piner RD, Nguyen ST, Ruoff RS (2006) Graphene-based composite materials. Nature 442:282

Strauss V, Marsh K, Kowal MD, ElKady M, Kaner KRB (2018) A simple route to porous graphene from carbon nanodots for supercapacitor applications. Adv Mater 30:1704449

Studer AM, Limbach LK, Van Duc L, Krumeich F, Athanassiou EK, Gerber LC, Moch H, Stark WJ (2010) Nanoparticle cytotoxicity depends on intracellular solubility: comparison of stabilized copper metal and degradable copper oxide nanoparticles. Toxicol Lett 197:169–174

Sutter P (2009) Epitaxial graphene: how silicon leaves the scene. Nat Mater 8:171

Tabish TA, Pranjol MZI, Horsell DW, Rahat AA, Whatmore JL, Winyard PG, Zhang S (2019) Graphene oxide-based targeting of extracellular cathepsin D and cathepsin L as a novel anti-metastatic enzyme cancer therapy. Cancers 11:319

Theivasanthi T, Alagar M (2010) X-ray diffraction studies of copper nanopowder. arXiv preprint arXiv 1003: 6068

Tuinstra F, Koenig JL (1970) Raman spectrum of graphite. J Chem Phys 53:1126–1130

Vallabani N, Mittal S, Shukla RK, Pandey AK, Dhakate SR, Pasricha R et al (2011) Toxicity of graphene in normal human lung cells (BEAS-2B). J Biomed Nanotechnol 7:106–107

Viswanathan A, Shetty AN (2018) Single step synthesis of rGO, copper oxide and polyaniline nanocomposites for high energy supercapacitors. Electrochim Acta 289:204–217

Wei L, Lu J, Xu H, Patel A, Chen ZS, Chen G (2015) Silver nanoparticles: synthesis, properties, and therapeutic applications. Drug Discov Today 20:595–601

Wojtoniszak M, Chen X, Kalenczuk RJ, Wajda A, Łapczuk J, Kurzewski M, Drozdzik M, Chu PK, Borowiak-Palen E (2012) Synthesis, dispersion, and cytocompatibility of graphene oxide and reduced graphene oxide. Colloids Surf B Biointer 89:79–85

Wu D, Yotnda P (2011) Production and detection of reactive oxygen species (ROS) in cancers. J Visual Exp Jove 57:3375

Xu H, Zeiger BW, Suslick KS (2013) Sonochemical synthesis of nanomaterials. Chem Soc Rev 42:2555–2567

Xu C, Shi X, Ji A, Shi L, Zhou C, Cui Y (2015) Fabrication and characteristics of reduced graphene oxide produced with different green reductants. PLoS ONE 10:e0144842

Yang Y, Asiri AM, Tang Z, Du D, Lin Y (2013) Graphene based materials for biomedical applications. Mater Today 16:365–373

Yang Y, Lu ZH, Hu Y, Zhang Z, Shi W, Chen X, Wang T (2014) Facile in situ synthesis of copper nanoparticles supported on reduced graphene oxide for hydrolytic dehydrogenation of ammonia borane. Rsc Adv 4:13749–13752

Yi M, Shen Z (2015) A review on mechanical exfoliation for the scalable production of graphene. J Mater Chem A 3:11700–11715

Yuan YG, Gurunathan S (2017) Combination of graphene oxide–silver nanoparticle nanocomposites and cisplatin enhances apoptosis and autophagy in human cervical cancer cells. Int J Nanomed 12:6537

Zhang B, Li L, Wang Z, Xie S, Zhang Y, Shen Y, Yu M, Deng B, Huang Q, Fan C (2012) Radiation induced reduction: an effective and clean route to synthesize functionalized graphene. J Mater Chem 22:7775–7781

Zhang J, Chen L, Shen B, Chen L, Mo J, Feng J (2019) A dual-sensitive graphene oxide loaded with proapoptotic peptides and anti-cancer drugs for cancer synergetic therapy. Langmuir 35(18):6120–6128

Zhao Y, Song X, Song Q, Yin Z (2012) A facile route to the synthesis copper oxide/reduced graphene oxide nanocomposites and electrochemical detection of catechol organic pollutant. Cryst Eng Comm 14:6710–6719

Zhao B, Liu P, Zhuang H, Jiao Z, Fang T, Xu W, Lu B, Jiang Y (2013) Hierarchical self-assembly of microscale leaf-like CuO on graphene sheets for high-performance electrochemical capacitors. J Mater Chem A 1:367–373